Hindawi
International Journal of Energy Research
Volume 2024, Article ID 9252190, 13 pages
https://doi.org/10.1155/2024/9252190

Research Article

Evaluation of Fe-Ni Composite Oxygen Carrier in Coal Chemical Looping Gasification

Kun Zhang[1,2] **and Qiumin Zhang**[2,3]

[1]*School of Chemical Engineering, Northeast Electric Power University, No. 169 Changchun Road, Jilin 132012, China*
[2]*Institute of Coal Chemical Engineering, School of Chemical Engineering, Dalian University of Technology, No. 2 Linggong Road, Dalian 116024, China*
[3]*State Key Laboratory of Fine Chemicals, Dalian University of Technology, No. 2 Linggong Road, Dalian 116024, China*

Correspondence should be addressed to Kun Zhang; zhangkun@neepu.edu.cn

Received 1 November 2023; Revised 12 January 2024; Accepted 9 February 2024; Published 23 February 2024

Academic Editor: Tholkappiyan Ramachandran

Although coal chemical looping gasification (CCLG) is a promising technology for the efficient utilization of coal, limited studies concerned about the industrial application of oxygen carrier in CCLG system owing to its performance requirements including high reactivity with solid fuel, high carbon conversion, and good mechanical property. To meet the requirements of oxygen carriers in CCLG system, novel Fe-Ni composite oxygen carrier (OC) samples were successfully prepared. The performances of these OCs were evaluated in a fixed bed reactor, where they were reduced by solid fuel and then fully oxidized by air. Both fixed bed tests and thermodynamic analysis showed that the prepare OCs exhibited high reactivity with coal and syngas selectivity, making them suitable for the CCLG process. Specifically, when the loading amount of NiO was 20 wt%, the Fe-Ni composite OCs achieved the highest carbon conversion (93.03%) and synthesis gas selectivity (73.29%). Additionally, the thermogravimetric data revealed that the Curie temperature of the OCs was higher than 550°C, making them suitable for magnetic separation of the OC particles and carbon residue in the CCLG system.

1. Introduction

Chemical looping gasification is an innovative gasification technology that splits the gasification process into two sequential reactions. It is usually accomplished by involving the use of oxygen carriers (OCs) that transport the needed oxygen from air to fuel, converting the fuel into fuel gas without the direct contact between oxygen and fuel. One of the main advantages of this gasification technology is that it avoids the cost and energy penalty of providing pure oxygen to the gasification system, thereby eliminating the dilution of N_2 and enhancing fuel gas calorific value [1]. Considering these unique features, there has been a growing interest in the study of chemical looping gasification, particularly in the area of OC development, as the availability of suitable OCs is considered a key issue for large-scale application of the technology [2, 3]. Most of the studies about chemical looping gasification focused on gas fuels such as methane while limited research concerned about the gasification of solid fuels [4–6]. The main reason is that chemical looping gasification of solid fuels has some drawbacks, such as low reaction rate, low conversion of solid fuel, and high mechanical strength requirements for OCs. However, China, a country rich in coal but lacking in crude oil and natural gas, cannot rely solely on gas-fueled chemical looping gasification to meet its energy demands. Therefore, it is necessary to actively develop coal chemical looping gasification (CCLG) technology, which uses coal as solid fuel. CCLG is a new coal utilization technology that achieves noncontact gasification of coal and air through the circulation of OC particles between the air reactor and fuel reactor, making it an effective way to achieve clean and efficient use of coal. Unlike conventional coal gasification technologies, which use molecular oxygen for direct oxidation, CCLG uses lattice oxygen in OCs for partial oxidation, converting coal into combustible gas [7]. Consequently, CCLG has great potential

to meet China's growing energy demands and reduce its dependence on imported fossil fuels. Considering the importance of OCs in CCLG development, further research is needed to develop suitable OCs to satisfy the performance requirement of OCs in CCLG system.

The simplified reaction mechanism and process of coal conversion in CCLG system are shown in Figure 1. Obviously, the CCLG system comprises two interconnected reactors: a fuel reactor and an air reactor. In the fuel reactor, coal is partially oxidized by oxidized OC particles to produce high-quality syngas. The reduced OC particles are then conveyed from the fuel reactor to the air reactor, where they are oxidized with the aid of air, thus achieving regeneration. As discussed above, the process of coal conversion in the fuel reactor involves the following reactions [8, 9]: (1) coal releases volatiles by thermal decomposition, (2) oxidized OC is reduced by released volatiles, (3) direct contact reaction between oxidized OC particles and coal, and (4) water-gas shift reaction between gaseous products. The reduced OC particles in the air reactor are reoxidized by air, and the regeneration process of OCs is expressed as follows: $Me + O_2 \rightarrow MeO$. Therefore, the performance of the CCLG system is largely determined by the properties of the OCs. Suitable OCs require high-temperature stability, great transportation ability of lattice oxygen, environmental friendliness, and low cost [10]. More importantly, in order to obtain a high-quality syngas, the OC samples should also present high reactivity with coal but weak reactivity with CO/H_2. Considering these desirable properties for OCs, the selection narrows towards several typical transition metals including Fe, Mn, Cu, Co, and Ni and their corresponding oxide systems. For instance, nickel oxides tend to sinter and agglomerate at high reaction temperatures, leading to the reduction of reactivity with solid fuel [11]. Among these metal transition oxides, Fe-based OCs have received a lot of attention because of low price, good recycling characteristics, and environmental friendliness [12]. Nevertheless, the low reactivity and poor mechanical properties of the Fe-based OCs have limited their application in the CCLG system. It was found that the addition of metal promoter could not only improve the reactivity of Fe-based OCs with coal but also produce a synergistic effect between the two metal oxides during the CCLG process [13]. More than that, the synergistic effect was help to improve the selectivity and yield of synthesis gas and enhance coal gasification during CCLG process. According to our previous study [14], Fe-based composite oxygen carrier with diverse metal promoters exhibited different gasification performance, and Fe-Ni composite oxygen carrier presented high carbon conversion of fuel and syngas selectivity in the CCLG process. Since the addition amount of metal promoter might be closely related to the gasification performance of OCs [15], the Fe-Ni composite OCs with varied NiO loadings were synthesized using microwave-assisted coprecipitation method and used for CCLG in this study. To further investigate the effect of addition amount of metal promoter Ni on the OC performance in the CCLG process, the reactivity of the prepared sample was tested in a fix bed reactor and the compositions of gas products including CH_4, CO_2, CO, and H_2 were measured by a gas chromatograph.

For the CCLG process, the solid residue after gasification is typically a mixture of reduced OCs and carbon residue, so it is necessary to separate the reduced OC particles from the carbon residue before the reduced OC particles are conveyed from the fuel reactor to the air reactor for regeneration. Ferromagnetic iron oxide is usually adopted in the chemical separation process due to its magnetic properties, which allow for effective separation of reduced OC particles from carbon residue by using magnetic separation. Compared with other separation methods, the magnetic separation has more advantages in reducing costs, saving energy, and reducing pollutants [16]. The OC particles with good magnetic properties contribute to effective magnetic separation from carbon residue in the CCLG process, and thus, the magnetic properties of the prepared samples were also investigated in this paper. It is widely acknowledged that the magnetic properties of materials are closely related to the operational temperature, and the magnetism of materials diminishes with the increase of operational temperature [17]. The Curie point is usually used for measuring the change in the magnetism of materials, and it is the temperature at which ferromagnetic iron oxide materials lose their intrinsic permanent magnetic properties [18]. Therefore, the Curie point gives an upper limit to the operational temperature for the magnetic media. In this study, to investigate the magnetic properties of OC samples synthesized by various NiO loadings, the Curie points of OCs were determined using thermomagnetic measurements.

2. Experimental

2.1. Preparation of the OC Particles. The Fe-based composite OC samples were synthesized using microwave-assisted coprecipitation method, and the synthesis steps were described in detail as follows. $Fe(NO_3)_3{\cdot}9H_2O$ and $Ni(NO_3)_2{\cdot}6H_2O$ were mixed thoroughly in the mass fraction of NiO = 0%, 5%, 10%, 15%, and 20% and followed by being dissolved in the diethylene glycol at 200°C in the microwave reactor for 30 min. After complete filtering and washing, the obtained solid precipitate was dried in an oven at 100°C for 12 h and then heated in a muffle furnace to 600°C at a heating rate of 3°C/min and held at 600°C for 6 h. To inhibit the agglomeration of the OC particles, 40 wt% of Al_2O_3 was added into the resulting calcined sample (Fe-Ni oxides) using the urea deposition–precipitation method. Therefore, the calcined sample and $Al(NO_3)_3{\cdot}6H_2O$ were mixed in the mass ratio of Al_2O_3 : Fe − Ni oxides = 2 : 3 and dissolved in deionized water. After complete mixing and stirring at 90°C, the obtained suspension liquid was washed twice with deionized water to remove traces of acid and urea. After drying at 100°C overnight, the resulting production was heated in a muffle furnace to 1000°C at the heating rate of 3°C/min and kept at 1000°C for 6 h. The composite OC samples with 20% (mass fraction) of NiO were denoted as 20%-OCs. The procedure for synthesizing OC samples with other mass fraction of NiO in composite, including 15%, 10%, 5%, and

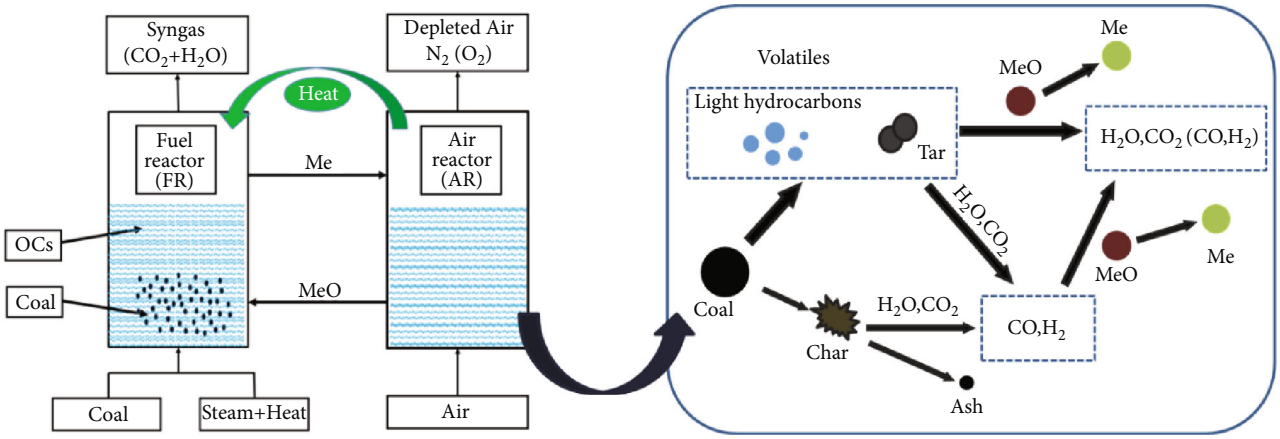

Figure 1: Illustration of the CCLG technology and coal conversion process.

0%, was essentially the same. The raw coal particles were dried in a vacuum oven at 105°C overnight and subsequently crushed and sieved to particles of size range 220–500 μm for experimentation. The proximate and ultimate analyses of coal samples are presented in Table 1.

2.2. OC Characterization. N_2 adsorption/desorption analysis (Micromeritics ASAP 2020) was carried out at 77 K for obtaining specific surface area and pore structure of the fresh and postreaction OCs. The specific surface area of Fe-based composited OCs could be obtained based on the adsorption isotherm by means of Brunauer–Emmett–Teller (BET) and pore structure of the samples including pore diameter and pore volume was also determined from the desorption isotherm according to Barret-Joyner-Halenda (BJH) method. Besides, X-ray diffraction (XRD), considered as a definitive technique to study the crystalline structures in a wide range of materials, was performed to identify crystalline phases of OC samples using an X-ray diffractometer in conjunction with Copper Kα radiation (40 kV, 40 mA). The samples were scanned in an angular range (2θ) of 5° to 80° with a rate of 0.02°/s. The surface morphologies of Fe-based composited OC samples were studied using a JEOL LSM-5400 SEM.

The Curie temperature of OC samples was studied in a thermogravimetric analysis (TGA) equipped with an Nd–Fe–B magnet ($100 \times 50 \times 5\,mm^3$) placed over the tested samples at a distance of about 10 cm OCs. In each test, about 15 mg Fe-based OC samples (<100 mesh) placed in an alumina crucible were heated from ambient temperature to 800°C at a heating rate of 10°C/min in argon (Ar) with a flow rate of 50 mL/min. When the temperature was lower than the Curie temperature of OC particles, the weights of OC particles recorded by TGA were less than their actual weights due to the magnetic attraction between the OC samples and magnet. With the increase of temperature, the magnetism of OC samples decreased gradually, and the weights of OC samples recorded by TGA increased gradually. When the temperature was higher than the Curie temperature of OC particles, the weights recorded by TGA were equal to their actual weight as the OC particles lose their magnetism. Generally, the Curie temperature of OC sample was the temperature corresponding to the maximum weight increase rate of the samples in the heating process [19].

2.3. Experiment Setup and Test Procedure. The fixed bed reactor setup, shown in Figure 2, was designed to provide information regarding the reactivity of Fe-based composite OCs with coal and the influence of OCs with various NiO loadings on product yields and gaseous composition. The fixed reactor was a quartz tube with an outer diameter of 27 mm, an inner diameter of 19 mm, and a length of 900 mm. Prior to each test, the samples including coal and OC particles were mixed thoroughly and the mixing ratio of coal and OCs was consistent with the stoichiometric oxygen supply to produce CO, with the fully reduction to metallic Ni and Fe [14]. For example, for Fe_2O_3, the stoichiometric reaction for coal was $Fe_2O_3 + 3C = 2Fe + 3CO$. In each experiment, about 3 g sample (coal–OC mixture) placed into quartz tube, heated by a heating furnace, whose temperature monitoring system on real time was realized based on a K-type thermocouple and PID controller. After removing air by introducing high purity N_2 with a flow rate of 100 mL/min, the mixture sample was heated by an electric furnace from room temperature to 800°C at a heating rate of 30°C/min. Subsequently, a proportion of steam was introduced with a N_2 stream to enhance the gasification while temperature was maintained at 800°C for 30 min. According to our previous study about the effect of steam concentration on product yields and gas composition, steam concentration of 15 vol% contributed to the maximum yield of synthesis gas and comparatively low yield of CO_2 [13]. Therefore, steam concentration of 15 vol%, controlled by a pump and an evaporator, was selected for gasification experiments, and the compositions of resulting gas (CO_2, H_2, CO, and CH_4) produced in the gasification step were real time analyzed with a gas chromatograph (GC-2010 Plus, SHIMADZU). After the gasification step, the flow gas was switched to air to combust residual coal at 800°C for 120 min and the gaseous products in oxidation step were also measured to calculate content of residual carbon in the solid residue. Furthermore, each test was repeated three times to ensure repeatability.

Table 1: Proximate and ultimate analyses of coal.

	Proximate analysis (wt%)				Ultimate analysis (wt%, daf)					$Q_{net,v,d}$ (MJ/kg)
	A_d	V_d	M	FC_d*	C	H	N	S	O*	
Coal	17.38	39.59	8.89	43.03	65.00	4.83	1.16	0.58	28.43	20.70

*By difference.

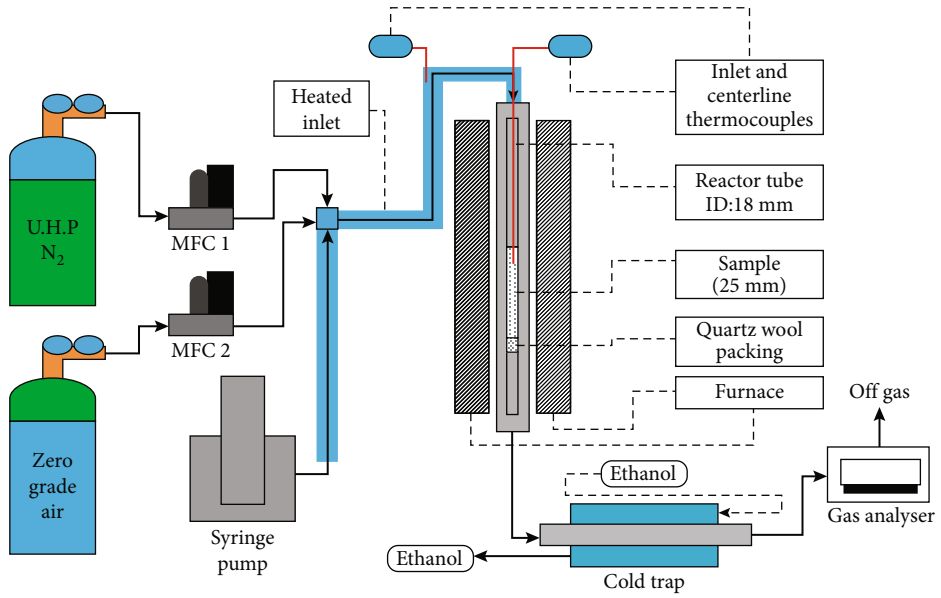

Figure 2: Schematic layout of fixed bed reactor.

To investigate the effect of OCs with different NiO loadings on total carbon conversion, the flow gas was switched to air after the gasification stage to oxidize the residual coal that was not gasified. Additionally, the evolved gas produced in the oxidation step was also analyzed to calculate carbon conversion and content of residual carbon. Carbon conversion (X_c) was defined as follows [14]:

$$X_C = \frac{V\left(x_{CO} + x_{CO_2} + x_{CH_4}\right)}{22.4 \times n_{C,Coal}}, \quad (1)$$

where x_{CO}, x_{CO2}, and x_{CH4} were the concentration of CO, CO_2, and CH_4 in the exhaust gas measured by gas chromatograph, respectively; V was the total gas volume collected during the oxidation process, including gas products and air; and $n_{C,Coal}$ was the mole contents of fixed carbon contained in the raw coal. As a result, the carbon conversion was the ratio of carbon content in the gaseous products to the total carbon content in the raw coal. Furthermore, the residual carbon (R_c) in the raw coal could be also calculated based on carbon balance:

$$R_c = 1 - X_c. \quad (2)$$

Apart from carbon conversion, the selectivity of synthesis gas was also important parameter to evaluate gasification performance of the prepared OCs. As a result, the synthesis gas selectivity (Sg) was discussed and calculated as [13]

$$Sg = \frac{x_{CO} + x_{H_2}}{x_{CO} + x_{CO_2} + x_{H_2} + x_{CH_4}}, \quad (3)$$

where x_{H_2} was the concentration of H_2 in the outlet gas stream measured by gas chromatograph. Obviously, Sg referred to the molar volume fraction of synthesis gas including CO and H_2 in gas products.

2.4. Thermodynamic Analysis. The change of the Gibbs free energy (ΔG) can be used as a criterion for the direction and limit of thermodynamic processes and as a measure of the magnitude of process irreversibility [20]. When ΔG was positive, indicating that the thermodynamic process was not thermodynamically feasible, and when ΔG was equal to zero, the thermodynamic process reached equilibrium; while ΔG was negative, the thermodynamic process was spontaneous, and the smaller the ΔG value was, the stronger the tendency of this thermodynamic process will be. The purpose of thermodynamic analysis was to clarify the possibility of the reaction between composite OCs and C/CO/H_2 and the relationship between the reaction tendency and temperature based on this criterion [21]. The ΔG values for potential reactions between C/CO/H_2 and composite OCs at different temperatures were calculated by adopting Aspen Plus software, which illustrated the dependency of ΔG on temperature for

reactions between C/CO/H_2 and composite OCs. Since the initial and final reduction products of Fe_2O_3 are Fe_3O_4 and Fe, respectively, and reaction ΔG of FeO formation was between that of Fe and Fe_3O_4 formations, FeO generation was not considered in the calculation of ΔG for reduction products of Fe_2O_3.

3. Results and Discussions

3.1. Thermodynamic Analysis Data with Coal and OCs. Figures 3(a) and 3(c) show the ΔG values for all possible reactions between carbon and the composite OCs. At temperature above 800°C, the ΔG values for these reactions can be ordered as $NiO > Fe_2O_3 > NiFe_2O_4$, indicating that $NiFe_2O_4$ was the easiest to be reduced by carbon, followed by Fe_2O_3 and NiO within the corresponding temperature range. Similarly, Figures 3(b) and 3(d) revealed that $NiFe_2O_4$ was the easiest to be reduced by H_2 and CO, followed by Fe_2O_3 and NiO. Consequently, $NiFe_2O_4$ had the strongest oxidation ability while NiO had the weakest oxidation ability among three active components in the Fe-Ni composite OCs. In addition, the reaction ΔG values for the initial and final reduction products of Fe_2O_3 reduced by carbon were negative at temperature higher than 400°C and 660°C, respectively. Consequently, Fe_2O_3 was thermodynamically feasible to react with carbon to generate CO at the temperature range of 400-1200°C. Similarly, $NiFe_2O_4$ and NiO were thermodynamically favorable to react with carbon to generate CO at temperature higher than 600°C, as indicated by the negative ΔG values for reactions between $NiFe_2O_4$/NiO and carbon. The ΔG values for potential reactions between CO/H_2 and composite OCs are shown in Figures 3(b) and 3(d). According to the ΔG values, Fe_2O_3 could be reduced to Fe_3O_4 by CO/H_2 at the whole temperature range. Furthermore, $NiFe_2O_4$ and NiO could react with CO and H_2, respectively, to generate CO_2 and H_2O in the temperature range of 400-1200°C. Overall, these results suggest that the prepared composite OCs were ideal choice for CCLG to produce synthesis gas from the viewpoint of thermodynamics.

3.2. Fixed Bed Reactor Tests

3.2.1. Gas Composition with Different NiO Loadings. To investigate the effect of NiO loadings in the prepared composite OCs on gasification performance, coal mixed with OC samples was heated in a fixed bed reactor from ambient temperature to 800°C at a heating rate of 30°C/min in N_2 with 15 vol% steam concentration. The compositions of resulting gas, including CO, H_2, CO_2, and CH_4 produced during the gasification process, were analyzed with a gas chromatograph, and the real-time concentration data is presented in Figure 4. It was remarkable that CH_4 concentration for prepared composite OCs with different NiO loadings exhibited similar trends. This mainly resulted from that most of CH_4 was produced by coal devolatilization during the CCLG process [22]. At the initial stage of the gasification process, CH_4 concentration increased dramatically and reached the peak value in about 10 minutes. Afterward, the amount of CH_4 continuously decreased, approaching zero in about 60 minutes with the consumption of carbon source in coal.

Although the real-time concentration data of CO, H_2, and CO_2 exhibited similar trends with CH_4, the time for CO, H_2, and CO_2 concentration to reach the peak value was different. It was evident from Figure 4 that the time for CO_2 concentration reach the peak was significantly shorter than that for CO concentration. This was mainly due to the selectively oxidation of the prepared composite OCs. It was known that there existed two types of oxygen species in OCs, including surface oxygen and bulk lattice oxygen. The gasification reaction between coal and OC particles occurred via surface oxygen and bulk lattice oxygen [23]. Surface oxygen tended to completely oxidize fuel and gaseous intermediates to CO_2 and H_2O due to its higher reactivity while lattice oxygen was prone to selective oxidation of fuel to produce CO in conjunction with H_2. Therefore, at the initial stage of the reaction, fuel and gaseous intermediates were completely oxidized to CO_2 and H_2O by surface oxygen in OCs, which was consistent with the conclusion obtained by concentrations of CO_2 during gasification processes. The results revealed the fact that the concentration of CO_2 rapidly reached its maximum and then gradually decreased due to the consumption of surface oxygen in OCs. Subsequently, fuel and gaseous intermediates were partially oxidized to CO by the lattice oxygen in OCs, resulting in CO concentration rapidly increased and reaching its peak value about 20 minutes, and then became decreasing as the lattice oxygen in OCs was consumed. Apart from the selective oxidation of fuel, the CO_2 yield might also be influenced by the water-gas shift reaction which had a positive effect on the generation of CO_2/H_2 and elimination of CO/H_2O. It was worth noting that there were approximate CO concentrations between 5%-OCs and 10%-OCs, which were evidently higher than that for 15%-OCs. Additionally, CO_2 concentration for 10%-OCs was significantly higher than that for OCs with other NiO loadings, which was not favorable for its application in CCLG process.

3.2.2. Gas Yield with Different NiO Loadings. To further evaluate the gasification properties of composite OCs with various NiO loadings, fixed bed tests were conducted using a 3 g sample containing OC and coal. The yields of gases including H_2, CO_2, CH_4, and CO produced during the CCLG process were analyzed, and the results are shown in Figure 5. Repeated tests with samples (coal–OC mixture) were also performed to assess the consistency of the results, and the variations of two repeated tests are presented in Figure 5. It was noteworthy that CH_4 yield was considerably lower than those of the other gases. Moreover, there were no significant differences in CH_4 yield across the different NiO loadings, whereas the CO_2 yields exhibited an opposite tendency. Specifically, the CO_2 yield for 10%-OCs was much higher than that for OCs with other NiO loadings, which was consistent with the gas composition data. Additionally, the yield of H_2 and CO was much lower for 0%-OCs than for other NiO loading OCs, suggesting that the addition of Ni was beneficial for achieving a higher yield of synthesis

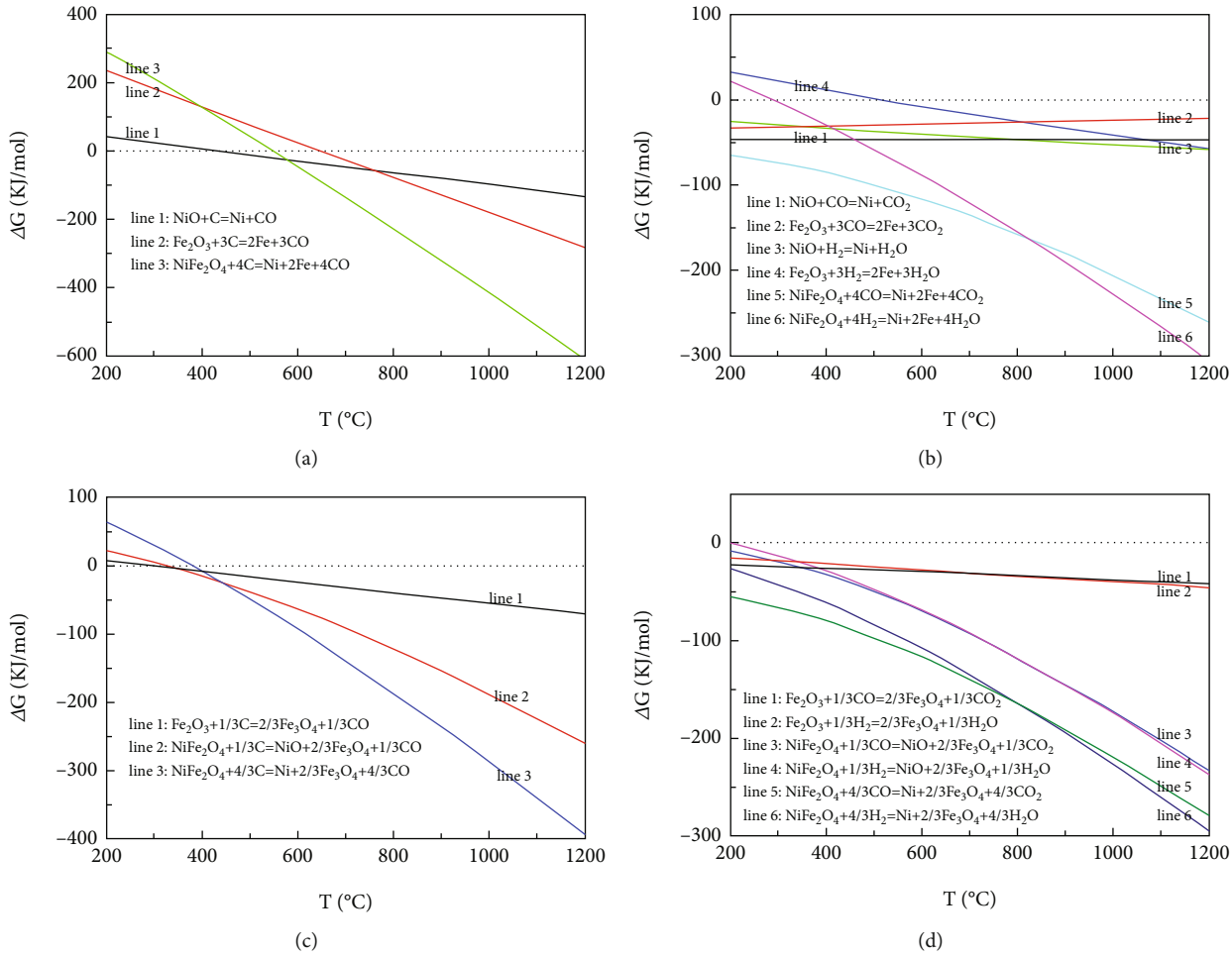

Figure 3: ΔG (kJ/mol) of the reactions between C/CO/H_2 and OCs.

gas. This might be attributed to the water-gas shift reaction, which resulted in an increase in the synthesis gas yield. Furthermore, several reactions might be involved in gasification process when composite OCs contained Fe and Ni, including methane decomposition and the direct solid-solid reaction between coal and composite OCs, which could also contribute to a higher yield of H_2 and CO [24]. However, when composite OCs with 20% NiO loadings were present, unlike the 10%-OCs, they had comparatively high yields of H_2 and CO and a relatively low CO_2 yield, making them a feasible choice for producing synthesis gas during the CCLG process.

3.2.3. Comparative Conversion and Selectivity with Different NiO Loadings. Table 2 reveals the fact that the contents of residual carbon were higher with 0%-OCs than with other NiO loading OCs, indicating that the addition of Ni contributed to achieving the full conversion. This might attribute to the interactions between iron oxide and metal promoter during gasification process. Moreover, the results clearly indicated that the amount of NiO loading had a significant effect on the carbon conversion of the fuel. It was worth noting that the carbon conversion for 20%-OCs was 93.03%, which was the highest among five NiO loading OCs. However, 0%-OCs achieved the lowest carbon conversion at 68.64%. Generally, the higher the carbon conversion of the fuel during the gasification process, the higher the reactivity of OCs with coal. Consequently, according to the total carbon conversion during gasification process, the reactivity of the five NiO loading OCs in the fixed bed reactor could be ranked as follows: 20%-OCs>5%-OCs>10%-OCs>15%-OCs>0%-OCs, which was in good agreement with the inference on the basis of gas composition data.

Table 2 shows the comparative synthesis gas selectivity of five NiO loading OCs during fixed bed tests. The loading amount of NiO was found to have a significant influence on the selectivity of synthesis gas in addition to carbon conversion of fuel. These data were very encouraging since 20%-OCs not only achieved the highest carbon conversion during gasification process but also had a relatively high selectivity of synthesis gas, which was 73.29%. The gaseous products mostly contained CO and H_2 when 20%-OCs were present during gasification process. This suggested that the reaction could be controlled to produce mainly synthesis gas without getting further oxidized to CO_2 and H_2O. Hence, the prepared composite OCs with 20% loadings were found suitable for various chemical processes for synthesis gas production. To understand the effect of NiO loadings, the selectivity of

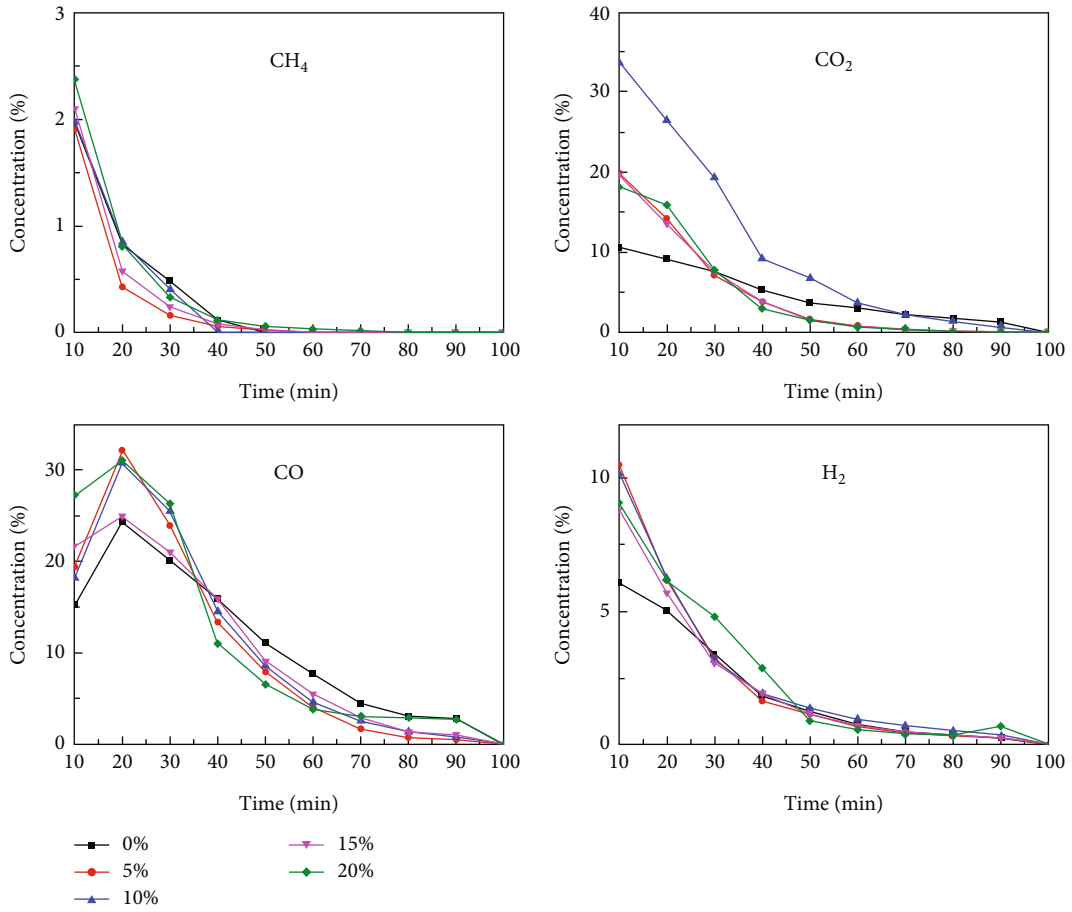

Figure 4: Real-time gas concentrations on coal gasification with composite oxygen carrier.

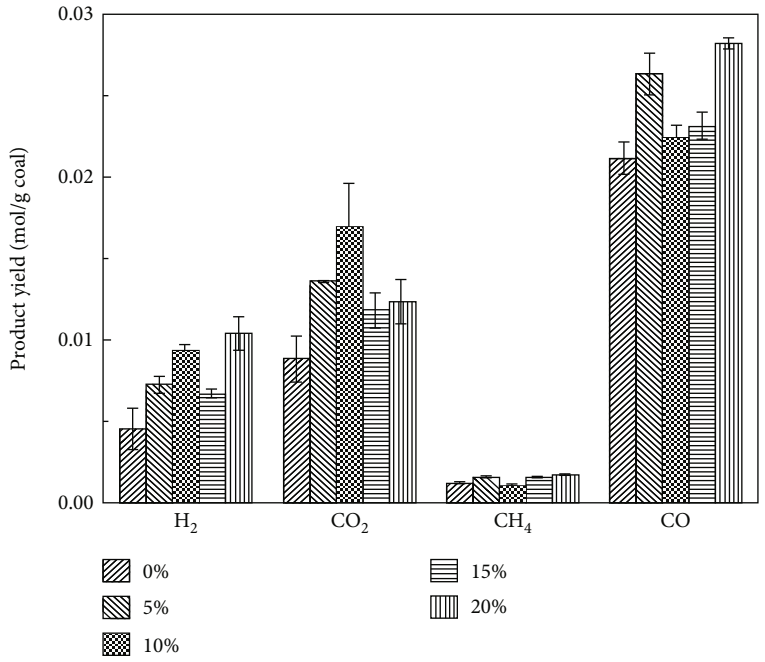

Figure 5: Gas yields on coal gasification with composite oxygen carrier.

Table 2: Effect of NiO loadings on carbon conversion of fuel and syngas selectivity.

NiO loading (wt%)	X_c (%)	R_c (%)	Sg (%)
0	68.64	31.36	71.91
5	91.29	8.71	68.81
10	88.78	11.22	60.25
15	80.34	19.66	69.05
20	93.03	6.97	73.29

synthesis gas for five NiO loading OCs during the gasification process could be ranked as follows: 20%-OCs>0%-OCs>15%-OCs>5%-OCs>10%-OCs.

3.3. Characteristic of OCs

3.3.1. Surface Area and Porosity Analysis of OCs. The specific surface area and pore structure of OCs were closely related to the dispersion of active sites and the accessibility of reactants to those sites [25]. Therefore, the surface area and pore structure of prepared OCs with varied NiO loadings are analyzed and listed in Table 3. The surface area of fresh Fe-Ni composite OCs was slightly higher than that of fresh Fe-based OCs. In general, the OC particles with larger pore volume and surface area contributed to more active sites and thus a higher reactivity with solid fuel during gasification process [26]. From this point of view, the addition of NiO had positive effects on improving reactivity of OCs with solid fuel [27]. Notably, the pore volumes of the fresh OC samples were relatively small and in the same order owing to high-temperature calcination treatment in the process of preparation of OCs [28]. Moreover, the loading amount of NiO significantly influenced pore size of fresh OCs. Among the five prepared OCs with different NiO loadings, 15%-OCs had the largest pore size, subsequently followed by 20%-OCs, 10%-OCs, 5%-OCs, and 0%-OCs, respectively. The surface area and pore structure of postreaction OCs were also analyzed and compared with those of fresh OCs. It could be concluded that the surface area of OCs became larger after gasification, whereas the pore size of postreaction OCs was smaller than that of fresh OCs. This might result from that the interactions between OC particles and reducing agent including gaseous intermediates and solid fuel during gasification process, which increased the number of micropores and led to an increase of surface area and reduction of average pore diameter [29]. Although the differences were observed in surface area and pore structure between fresh and postreaction OCs, the OC particles after reaction still remained relatively large pore volume and surface area, which was very favorable for their application in CCLG system.

3.3.2. XRD Analysis of OCs. Figure 6 shows the XRD patterns of five NiO loading OCs after reduction and oxidation at 800°C and compares with the raw samples. The XRD data of the OC samples before testing revealed that the active component of OCs without NiO was Fe_2O_3, while OCs with NiO addition also contained NiO and $NiFe_2O_4$ in addition to Fe_2O_3. This might result from that the addition of metal promoter Ni disrupted part of crystalline lattice of Fe_2O_3, resulting in distortion of crystal lattice and simultaneous formation of iron-nickel solid solution [30]. XRD data of the 0%-OCs after reduction indicated the presence of Fe_3O_4 and Fe_2O_3 phases, as shown in Figure 6(a). However, for the Fe-Ni composite OCs after reduction, only the characteristic peaks of Fe_3O_4 and $NiFe_2O_4$ were detected in the XRD spectrogram, with no Fe_2O_3 characteristic peak presented. These data suggested that composite OCs were easier to be reduced with the addition of NiO during gasification process, which was benefit for improving reactivity of OCs with solid fuel. Notably, the characteristic peaks of FeO and Fe were not detected in the OC sample after reduction. This was mainly due to the fact that the conversion process of iron oxides in the OC samples was primarily $Fe_2O_3 \rightarrow Fe_3O_4$ during the gasification process. Additionally, the small amount of produced FeO and Fe could further react with water vapor to generate Fe_3O_4, as steam was introduced into the fixed bed reactor [31]. Based on these analyses, iron oxides in composite OCs had the following conversion:

$$\begin{aligned} Fe + H_2O &\longrightarrow Fe_3O_4 + H_2 \\ FeO + H_2O &\longrightarrow Fe_3O_4 + H_2 \end{aligned} \quad (4)$$

To evaluate the cycle performance of the tested OCs, the crystal form evolutions of five NiO loading OCs at different reaction stage were analyzed using XRD and compared with OCs before test, as shown in Figure 6. XRD data of fresh OCs without NiO revealed the presences of Fe_2O_3 phase, as shown in Figure 6(a). After a complete cycle of reduction and oxidation, the XRD spectrogram of 0%-OCs was similar to the fresh sample, indicating the potential for OC regeneration. When OCs with NiO addition were oxidized (oxidation with air) after gasification with coal, the main components were still Fe_2O_3, NiO, and $NiFe_2O_4$, indicating that the original phases were reformed after a complete cycle of reduction and oxidation. Therefore, it could be concluded that there was no change in the composition of the five NiO loading OCs since the fixed bed reactor tests were ended after a complete contact with air. However, it could be observed that the intense peaks showed a slight difference between fresh OCs and samples after redox cycle, and the characteristic peak intensity of fresh OCs was smaller than that of OCs after cycling. This is mainly due to the increase in the particle size and degree of crystallization of OCs after a full cycle of gasification and oxidation [32]. Nevertheless, there was no change in the material phases of the five NiO loading OCs after cycling compared with fresh OCs, suggesting that the prepared OCs were suitable for the cyclic test. More importantly, the results revealed the fact that NiO did not escape from composite OCs after a complete cycle of reduction and oxidation, which further confirmed previous conclusion that the addition of Ni disrupted part of crystalline lattice of Fe_2O_3 and simultaneously formed iron-nickel solid solution.

Table 3: Surface area and porosity analysis of oxygen carrier before and after reaction.

NiO loading (wt%)	S_{BET} (m^2/g)		Pore volume (cc/g)		Pore size (nm)	
	Fresh	Postreaction	Fresh	Postreaction	Fresh	Postreaction
0	2.45	7.03	0.01	0.02	6.19	4.27
5	2.51	8.77	0.01	0.02	9.53	5.53
10	2.85	9.50	0.01	0.03	10.41	6.97
15	2.99	10.71	0.01	0.02	13.13	7.34
20	2.92	13.22	0.01	0.02	11.02	6.87

3.3.3. Morphological Analysis of OCs. As shown in Figure 7, the SEM images of five NiO loading OCs after reaction were analyzed and compared with the fresh samples. Figures 7(a)–7(e) depict the morphology of fresh OC samples. Clearly, the fresh OC particles were featured by irregular shape. Additionally, the fresh 0%-OC particles exhibited relatively compact physical structure while the fresh Fe-Ni composite OC samples showed comparatively loose surface condition. Generally, the OC particles with comparatively loose physical structure contributed to relatively large surface area. Therefore, the addition of NiO was beneficial for Fe-based OCs to achieve larger surface area, which was consistent with the inference based on BET data. More importantly, there was barely any pore structure on the surface of fresh 0%-OCs, whereas the fresh Fe-Ni composite OC particles contained well-developed porous structure and part of particles cracked. Generally, the compact physical structure of OC particles was not conducive to the gaseous components entering the inner channel to react with the active components, and gas products could not be discharged in a timely manner [33]. Therefore, insufficient contact of solid fuel and OC particles was an important reason for the decrease in gasification activity of OC samples, which was verified by the XRD spectrum that 0%-OCs after gasification remained Fe_2O_3 phase. By comparing the morphology of fresh OCs with different NiO loadings, it could be concluded that the addition of NiO enhanced the reactivity of OCs with solid fuel by improving pore structures of the OC particles.

As shown in Figures 7(f)–7(j), the OC particles after gasification became smaller in size and rougher on surface but presented more abundant pore structures compared with fresh OC samples. The possible reason was that the lattice oxygen located in equilibrium positions of the lattice structure randomly transferred to the contacted particle interface during gasification process, thus forming an irregular structure with different grain sizes [34]. Actually, OC particles with porous structure were beneficial for the diffusion of reactants and enhancement of the gasification reaction. From this point of view, the OC sample exhibited a good heat-resistant properties as particles retained their pore structures after gasification. Moreover, there were no significant changes in the particle morphology between the regenerated and fresh OCs with NiO addition since the OC samples after gasification were oxidized with air atmosphere to recover the lattice oxygen completely. However, 0%-OC particles were crushed into small grain particles under identical conditions owing to their poor mechanical strength. The surfaces of the 0%-OC particles after a complete cycle of reduction and oxidation were quite rough, yet no pores were found on the surface of an individual grain. Furthermore, the particle morphology and porous structure of regenerated 5%-OCs and 20%-OCs (Figures 7(l) and 7(o)) were basically consistent with fresh samples, which was conducive to keeping stable performance for the cyclic tests. However, the SEM images of the 10%-OC samples after oxidation (Figure 7(m)) clearly showed a change in morphology compared with the fresh sample. This might result from that mineral matter in coal, such as alkali metal, which caused pore blockage and formation of larger agglomerates [35]. Nevertheless, there were no significant changes in the crystalline structures between the regenerated and fresh 10%-OCs according to previous analyses based on the XRD spectrum. Combined with the XRD data of OC samples, it could be concluded that the synthesized OCs with NiO addition were suitable for application in the gasification process without significant aggregation or reactivity deterioration.

3.3.4. Curie Temperature of OCs. To investigate effect of the loading amount of NiO on magnetic properties of OC samples, the Curie temperatures of fresh and postreaction OC samples were analyzed using thermomagnetic measurements. The TG and DTG curves of the fresh OC samples with different NiO loadings are shown in Figure 8. It was evident that the weight of 0%-OC samples almost did not change with the temperature increase from ambient to 800°C, owing to their weak magnetism. In contrast, significant changes in the weights of OC samples with NiO addition were observed, resulting from their magnetic properties sharply decreasing during heating process. The major weight change occurred in the temperature range of 550–650°C, during which the OC samples achieved the maximum rate of weight increase. Of the tested OC samples with NiO addition, 20%-OCs exhibited the maximum rate of weight increase, owing to the interaction of iron-nickel mixed metal oxide OCs, leading to the enhancement of magnetism [36]. Additionally, the characteristic temperature of 20%-OCs, corresponding to the maximum weight increase rate, was higher than that of the other OC samples. Based on the TG and DTG curves of fresh OC samples, the Curie temperature of five fresh OC samples could be concluded in the order of 20%-OCs>10%-OCs>15%-OCs>5%-OCs>0%-OCs. The TG and DTG curves of OC samples after gasification are also shown in Figure 9. It was worth noting that a significant difference in TG and DTG curves between fresh and postreaction OC samples was observed, suggesting that the magnetism of five NiO loading OCs changed substantially after gasification,

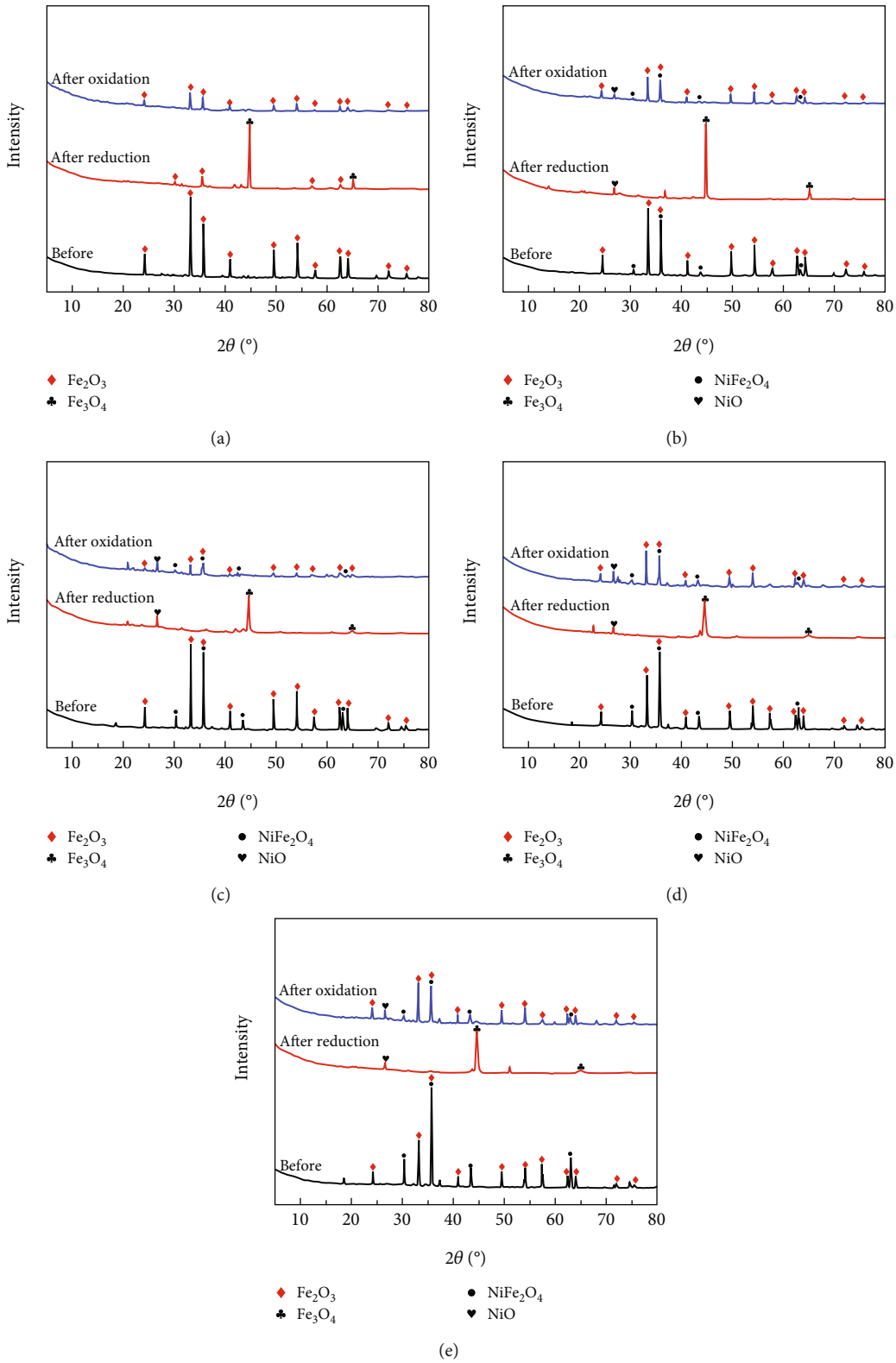

Figure 6: XRD patterns of oxygen carrier before and after reaction: (a) 0%; (b) 5%; (c) 10%; (d) 15%; (e) 20%.

especially the magnetism of 0%-OCs, which was obviously enhanced compared with that of fresh 0%-OCs. This resulted from that the conversion process of iron oxides in 0%-OCs, which was mainly $Fe_2O_3 \rightarrow Fe_3O_4$ during the gasification process, resulting in Fe_2O_3 in 0%-OCs being reduced to Fe_3O_4 with stronger magnetism [37]. Moreover, the magnetism of the other four OC samples after gasification was also improved to some extent due to the effect of iron oxides conversion.

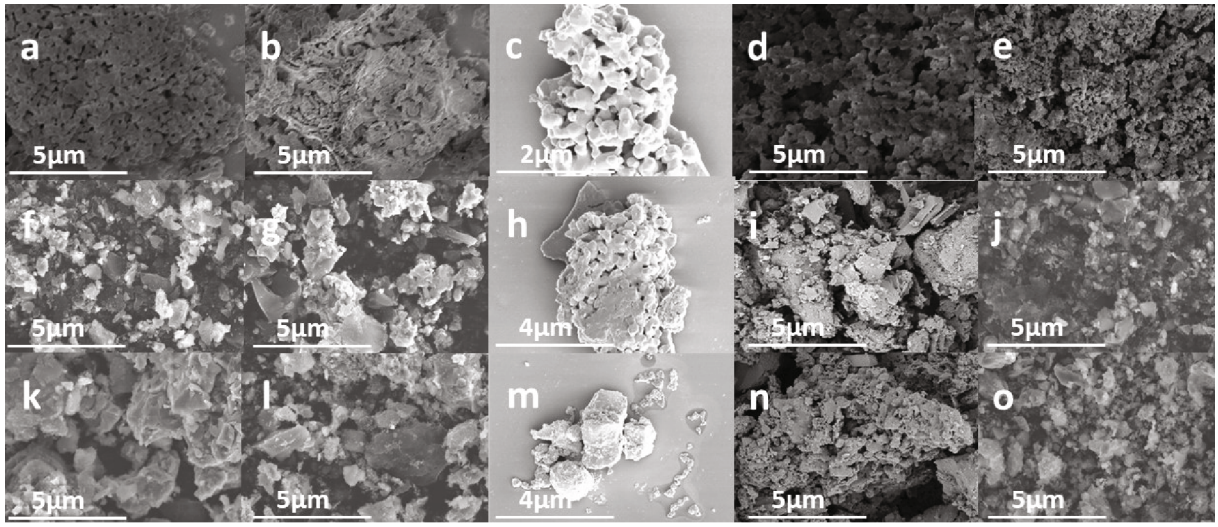

Figure 7: SEM images of the oxygen carrier before ((a) 0%; (b) 5%; (c) 10%; (d) 15%; (e) 20%) and after gasification ((f) 0%; (g) 5%; (h) 10%; (i) 15%; (j) 20%) and oxidation ((k) 0%; (l) 5%; (m) 10%; (n) 15%; (o) 20%) reaction.

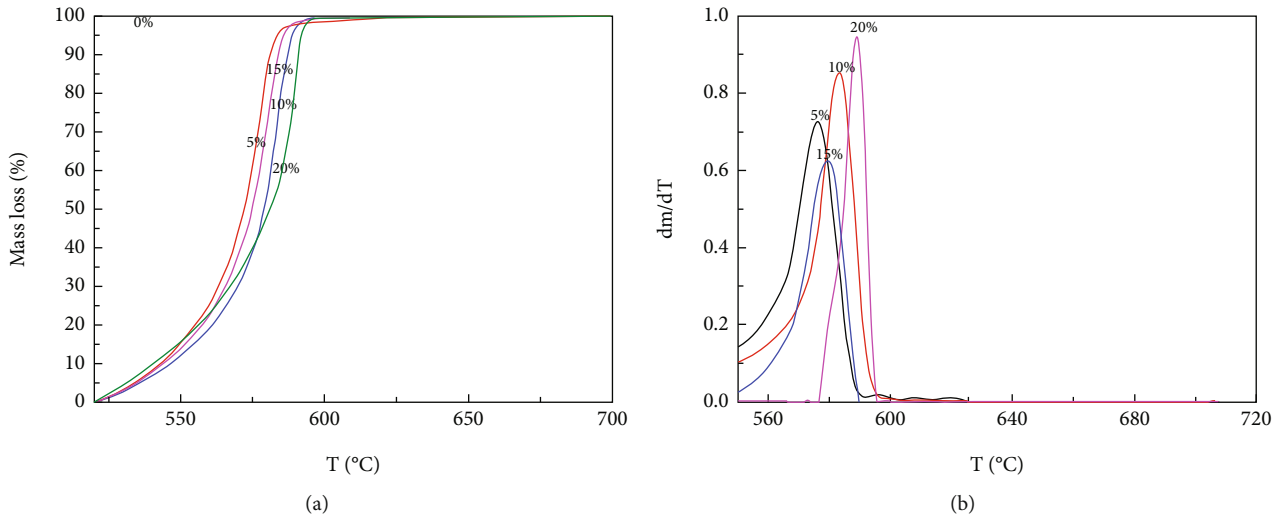

Figure 8: TGA and DTG curves of fresh oxygen carrier: (a) mass loss; (b) mass loss rate.

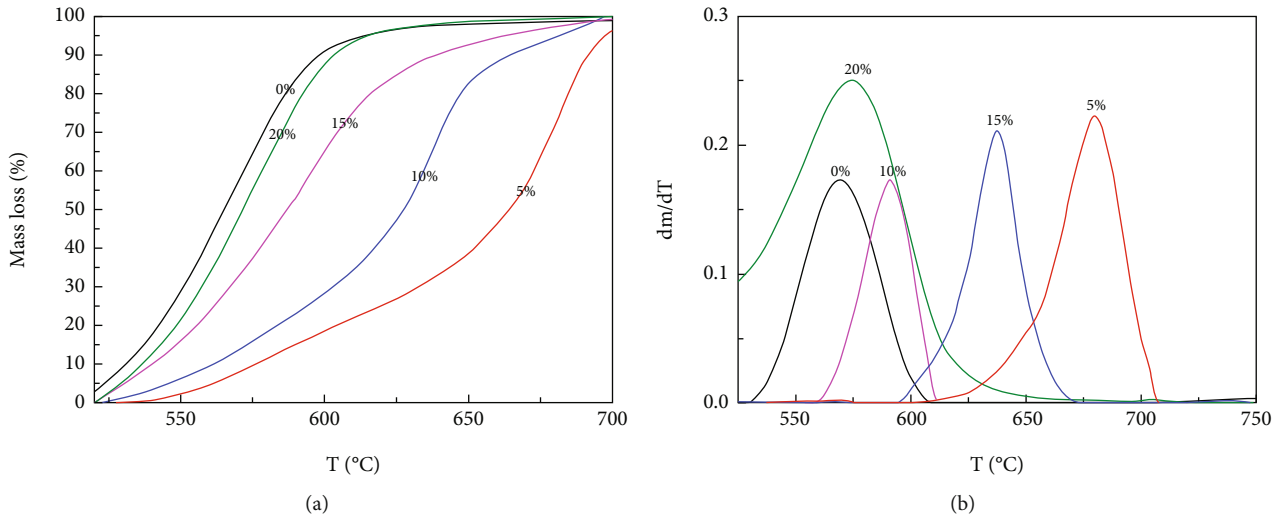

Figure 9: TGA and DTG curves of oxygen carrier after gasification: (a) mass loss; (b) mass loss rate.

Table 4: The Curie point of fresh and postreaction oxygen carrier.

NiO loading (wt%)	Fresh (°C)	Postreaction (°C)
0	—	570
5	577	680
10	583	591
15	580	637
20	589	573

Based on the TG and DTG curves, we concluded the Curie temperatures of fresh and postreaction OC samples, which are listed in Table 4. It should be mentioned that in addition to magnetic properties, the loading amount of NiO had a significant influence on the Curie temperature of OC samples. Among the five fresh OC samples, 20%-OCs exhibited the highest Curie temperature, close to 589°C, making it favorable for application in the separation of OC particles from carbon residue. However, for OC samples after gasification, 5%-OCs obtained the highest Curie temperature, close to 680°C. The Curie temperatures of the five postreaction OC samples could be concluded in the order of 5%-OCs>15%-OCs>10%-OCs>20%-OCs>0%-OCs. In general, among the five OC samples, except for OCs without adding NiO, the Curie points of the other four composite OCs before and after gasification were higher than 550°C, meeting the requirement of magnetic separation of OC particles.

4. Conclusions

In this work, Fe-based composite OC samples were successfully synthesized using microwave-assisted coprecipitation method, with the addition of Ni as a metal promoter. The effect of varying amounts of NiO on the gasification performance of OCs was analyzed using a fixed bed reactor. The Curie temperature, pore structure, and crystal structure of fresh and postreaction OCs were characterized using TGA, BET, SEM, and XRD. Such conclusions have been drawn as follows:

(1) Fix bed data and thermodynamics results indicated the addition of NiO significantly enhanced the reactivity and stability of Fe-based composite OCs during gasification. This was likely due to the addition of disruption of the crystalline lattice of Fe_2O_3 by the addition of NiO, resulting in a distortion of the crystal lattice and the formation of an iron-nickel solid solution as evidenced by XRD analysis

(2) The amount of NiO loading had a significant impact on the distribution of gas products, selectivity of syngas, and carbon conversion of fuel during the CCLG process. Fe-Ni composite OCs achieved the highest carbon conversion (93.03%) and synthesis gas selectivity (73.29%) when the loading amount of NiO was 20 wt%

(3) The addition of NiO greatly improved the magnetic properties of Fe-based composite OCs. The thermogravimetric data revealed that, except for OCs without NiO, the Curie temperatures of both fresh and postreaction OC samples were higher than 550°C, meeting the requirements for magnetic separation of OC particles and carbon residue in the CCLG system

Data Availability

The authors confirm that the data supporting the findings of this study are available within the article.

Conflicts of Interest

The authors declare that they have no conflicts of interest.

Acknowledgments

Support from the National Key R&D Program of China (2016YFB0600400) is greatly acknowledged.

References

[1] S. Haider, G. Azimi, L. Duan et al., "Enhancing properties of iron and manganese ores as oxygen carriers for chemical looping processes by dry impregnation," *Applied Energy*, vol. 163, pp. 41–50, 2016.

[2] S. Liang, Y. Liao, W. Li, C. Li, and X. Ma, "Enhanced stability of iron-nickel oxygen carriers in biomass chemical looping gasification by core-shell structure," *Chemical Engineering Journal*, vol. 451, article 138964, 2023.

[3] S. Liu, F. He, K. Zhao et al., "Long-term coal chemical looping gasification using a bimetallic oxygen carrier of natural hematite and copper ore," *Fuel*, vol. 309, p. 122106, 2022.

[4] J. Udomsirichakorn and P. A. Salam, "Review of hydrogen-enriched gas production from steam gasification of biomass: the prospect of CaO-based chemical looping gasification," *Renewable and Sustainable Energy Reviews*, vol. 30, pp. 565–579, 2014.

[5] F. Li, L. Zeng, L. Velazquez-Vargas, Z. Yoscovits, and L. S. Fan, "Syngas chemical looping gasification process: bench-scale studies and reactor simulations," *AIChE Journal*, vol. 56, no. 8, pp. 2186–2199, 2010.

[6] V. Shah, Z. Cheng, D. Baser, J. A. Fan, and L.-S. Fan, "Highly selective production of syngas from chemical looping reforming of methane with CO_2 utilization on MgO-supported calcium ferrite redox materials," *Applied Energy*, vol. 282, article 116111, 2021.

[7] H. Zhou, W. Meng, D. Wang et al., "A novel coal chemical looping gasification scheme for synthetic natural gas with low energy consumption for CO_2 capture: modelling, parameters optimization, and performance analysis," *Energy*, vol. 225, p. 120249, 2021.

[8] Q. Pan, L. Ma, W. Du et al., "Hydrogen-enriched syngas production by lignite chemical looping gasification with composite oxygen carriers of phosphogypsum and steel slag," *Energy*, vol. 241, p. 122927, 2022.

[9] D. D. Miller and R. Siriwardane, "$CaFe_2O_4$ oxygen carrier characterization during the partial oxidation of coal in the chemical looping gasification application," *Applied Energy*, vol. 224, pp. 708–716, 2018.

[10] Z. Huang, N. Gao, Y. Lin et al., "Exploring the migration and transformation of lattice oxygen during chemical looping with $NiFe_2O_4$ oxygen carrier," *Chemical Engineering Journal*, vol. 429, p. 132064, 2022.

[11] G. Wei, F. He, Z. Zhao et al., "Performance of Fe–Ni bimetallic oxygen carriers for chemical looping gasification of biomass in a 10 kWth interconnected circulating fluidized bed reactor," *International Journal of Hydrogen Energy*, vol. 40, no. 46, pp. 16021–16032, 2015.

[12] Q. Guo, Y. Cheng, M. Fan, Y. Liu, W. Jia, and H.-J. Ryu, "Coal chemical looping gasification for syngas generation using an iron-based oxygen carrier," *Industrial & Engineering Chemistry Research*, vol. 53, no. 1, pp. 78–86, 2014.

[13] Z. Kun, D. He, J. Guan, L. Shan, Z. Wu, and Q. Zhang, "Coal gasification using chemical looping with varied metal oxides as oxygen carriers," *International Journal of Hydrogen Energy*, vol. 45, no. 18, pp. 10696–10708, 2020.

[14] Z. Kun, D. He, J. Guan et al., "Interaction between bimetallic composite oxygen carriers and coal and its contribution to coal direct chemical looping gasification," *International Journal of Hydrogen Energy*, vol. 45, no. 38, pp. 19052–19066, 2020.

[15] A. Hafizi, M. Rahimpour, and S. Hassanajili, "Hydrogen production via chemical looping steam methane reforming process: effect of cerium and calcium promoters on the performance of Fe_2O_3/Al_2O_3 oxygen carrier," *Applied Energy*, vol. 165, pp. 685–694, 2016.

[16] M. Can, M. Coşkun, and T. Fırat, "A comparative study of nanosized iron oxide particles; magnetite (Fe_3O_4), maghemite (γ-Fe_2O_3) and hematite (α-Fe_2O_3), using ferromagnetic resonance," *Journal of Alloys and Compounds*, vol. 542, pp. 241–247, 2012.

[17] J. S. Kouvel and M. E. Fisher, "Detailed magnetic behavior of nickel near its Curie point," *Physical Review*, vol. 136, no. 6A, pp. A1626–A1632, 1964.

[18] G. Ferk, M. Drofenik, D. Lisjak, A. Hamler, Z. Jagličić, and D. Makovec, "Synthesis and characterization of $Mg_{1+x}Fe_{2-2x}Ti_xO_4$ nanoparticles with an adjustable Curie point," *Journal of Magnetism and Magnetic Materials*, vol. 350, pp. 124–128, 2014.

[19] W. Zhang, X. Zuo, Y. Niu et al., "Novel nanoparticles with Cr(3+) substituted ferrite for self-regulating temperature hyperthermia," *Nanoscale*, vol. 9, no. 37, pp. 13929–13937, 2017.

[20] J. Zhang, T. He, Z. Wang et al., "The search of proper oxygen carriers for chemical looping partial oxidation of carbon," *Applied Energy*, vol. 190, pp. 1119–1125, 2017.

[21] G. Liu, Y. Liao, Y. Wu, and X. Ma, "Application of calcium ferrites as oxygen carriers for microalgae chemical looping gasification," *Energy Conversion and Management*, vol. 160, pp. 262–272, 2018.

[22] L. Zeng, F. He, F. Li, and L. S. Fan, "Coal-direct chemical looping gasification for hydrogen production: reactor modeling and process simulation," *Energy & Fuels*, vol. 26, no. 6, pp. 3680–3690, 2012.

[23] Y. Lin, H. Wang, Y. Wang et al., "Review of biomass chemical looping gasification in China," *Fuels*, vol. 34, no. 7, pp. 7847–7862, 2020.

[24] L. Chen, J. Bao, L. Kong et al., "The direct solid-solid reaction between coal char and iron-based oxygen carrier and its contribution to solid-fueled chemical looping combustion," *Applied Energy*, vol. 184, pp. 9–18, 2016.

[25] H. Zhang, S. Shao, G. Ryabov, Y. Jiang, and R. Xiao, "Functional group in situ evolution principles of produced solid and product distribution in biomass torrefaction process," *Energy & Fuels*, vol. 31, no. 12, pp. 13639–13646, 2017.

[26] S. Liu, F. He, Z. Huang et al., "Screening of $NiFe_2O_4$ nanoparticles as oxygen carrier in chemical looping hydrogen production," *Energy & Fuels*, vol. 30, no. 5, pp. 4251–4262, 2016.

[27] N. M. Nguyen, F. Alobaid, P. Dieringer, and B. Epple, "Biomass-based chemical looping gasification: overview and recent developments," *Applied Sciences*, vol. 11, no. 15, p. 7069, 2021.

[28] J. Adánez, L. F. de Diego, F. García-Labiano, P. Gayán, A. Abad, and J. M. Palacios, "Selection of oxygen carriers for chemical-looping combustion," *Energy & Fuels*, vol. 18, no. 2, pp. 371–377, 2004.

[29] Z. Miao, L. Shen, Z. Li, and T. Shen, "Sintering and agglomeration characteristics of industrially prepared $CaMn_{0.5}Ti_{0.375}Fe_{0.125}O_{3-\delta}$ perovskite oxygen carrier in chemical looping combustion," *Chemical Engineering Journal*, vol. 472, article 144722, 2023.

[30] S. Bhavsar and G. Veser, "Bimetallic Fe–Ni oxygen carriers for chemical looping combustion," *Industrial & Engineering Chemistry Research*, vol. 52, no. 44, pp. 15342–15352, 2013.

[31] H. Leion, E. Jerndal, B.-M. Steenari et al., "Solid fuels in chemical-looping combustion using oxide scale and unprocessed iron ore as oxygen carriers," *Fuel*, vol. 88, no. 10, pp. 1945–1954, 2009.

[32] V. Shah, P. Mohapatra, and L. S. Fan, "Thermodynamic and process analyses of syngas production using chemical looping reforming assisted by flexible dicalcium ferrite-based oxygen carrier regeneration," *Energy & Fuels*, vol. 34, no. 5, pp. 6490–6500, 2020.

[33] B. M. Corbella, L. De Diego, F. García-Labiano, J. Adánez, and J. M. Palacios, "Characterization and performance in a multicycle test in a fixed-bed reactor of silica-supported copper oxide as oxygen carrier for chemical-looping combustion of methane," *Energy & Fuels*, vol. 20, pp. 148–154, 2006.

[34] L. Protasova and F. Snijkers, "Recent developments in oxygen carrier materials for hydrogen production via chemical looping processes," *Fuel*, vol. 181, pp. 75–93, 2016.

[35] Z. Ma, J. Wang, G. Liu et al., "Regeneration of deactivated Fe_2O_3/Al_2O_3 oxygen carrier via alkali metal doping in chemical looping combustion," *Fuel Processing Technology*, vol. 220, article 106902, 2021.

[36] S. Ldsco and F. L. Roftlsd, "Determining the curie temperature of iron and nickel," *The Physics Teacher*, vol. 45, no. 6, pp. 387–389, 2007.

[37] M. Shi, P. Zhang, M. Fan, P. Jiang, and Y. Dong, "Influence of crystal of Fe_2O_3 in magnetism and activity of nanoparticle $CaO@Fe_2O_3$ for biodiesel production," *Fuel*, vol. 197, pp. 343–347, 2017.